Orthotropic mechanical properties of Fused Deposition Modelling parts described by Classical Laminate Theory

Orthotropic mechanical properties of Fused Deposition Modelling parts described by Classical Laminate Theory

Caterina Casavola[1], Alberto Cazzato[1], Vincenzo Moramarco[1,*] and Carmine Pappalettere[1]
[1]Dipartimento di Meccanica, Matematica e Management (DMMM) - Politecnico di Bari - Viale Japigia 182 - 70126 Bari (Italy)
*phone +39 080 596 2830; fax +39 080 596 2777; e-mail vincenzo.moramarco@poliba.it

Abstract

The Fused Deposition Modelling (FDM) has become one of the most used techniques to 3D object rapid prototyping. In this process, the model is built as a layer-by-layer deposition of a feedstock wire. In recent years, the FDM evolved from rapid prototyping technique towards a rapid manufacturing method, changing the main purpose in producing finished components ready for use. Thus, the prediction of the mechanical properties of this new technology has an increasingly important role. Previous papers have highlighted the orthotropic mechanical behaviour of FDM parts showing that the stacking sequence controls the mechanical properties of FDM parts. The aim of this work is to describe the mechanical behaviour of FDM parts by the classical laminate theory (CLT). In order to reach this objective, the values of the elastic modulus in the longitudinal and transverse directions to the fibre (E_1, E_2), the Poisson's modulus (ν_{12}) and the shear modulus (G_{12}) will be experimentally measured.

Keywords: fused deposition modelling; classical laminate theory; orthotropic mechanical behavior; mechanical characterization.

1. Introduction

The Fused Deposition Modelling (FDM), developed by Stratasys Inc., has become one of the most used techniques to 3D object rapid prototyping. This technology has many potential fields where it could be used, however, the currently main applications are the design verification, kinematic functionality testing, fabrication of models for visualization and medical applications [1]. In this process, as for many others 3D printing technologies [2], the model is built as a layer-by-layer deposition of a feedstock material. Initially, the raw material is in the form of filament that is partially melted, extruded and deposited by a heated nozzle onto the previously built model [3]. After the deposition, the material cools, solidifies and sticks with the surrounding material. Once the entire layer has been deposited, the nozzle moves upward along the z-axis for the deposition of the next layer. The principle of the FDM technology offers great potential because, without any need for machining, allows the fabrication of complex 3D parts directly from a computerized solid model. Traditionally, the FDM 3D printers have been able to build parts only in thermoplastic materials such as polylactic acid

(PLA) and acrilonitrile-butadiene-stirene (ABS). The PLA offers better thermo-mechanical characteristics than ABS having a stronger mechanical resistance and a lower coefficient of thermal expansion. The last characteristic improves the printability of PLA because reduces the effects of warping during the printing phase. Moreover, it shows less health risks than ABS when printing in small and improperly ventilated spaces [4]. Nowadays, many others materials have been used or developed, e.g., bioresorbable polymer (PCL) [5], short fibre composites [6], ceramics [7], metal [8] and metal/polymers mixture materials [9].

In recent years, the FDM evolved from rapid prototyping technique towards a rapid manufacturing method, changing the main purpose in producing finished components ready for use [1, 10]. Indeed, this technique is particularly promising for the fabrication of a single piece or, in general, low volume products such as replacement parts for not widespread system. This trend highlights the need for a deep understanding of the mechanical properties and the behaviour of parts produced by FDM. A thorough understanding of the mechanical properties is complex, because this is influenced by many production parameters whose combination is often difficult to understand. Moreover, a FDM part can be considered as laminated composite structure with vertically stacked layers of bonded fibres [11]. As consequence, not only the feedstock material controls the mechanical properties of FDM parts, but also, the stack sequences whereby the layers are overlapped. Several papers deal with the anisotropic characteristics of FDM parts in recent years. Ahn et al. [11] carried out several experiments to determine the effects of air gap, bead width, raster orientation and ABS colour on tensile and compressive strengths. They determine that air gap and raster orientation have an important effect on the tensile strength, on the other hand, the other parameters have negligible effects. Moreover, the factors that they have studied do not affect the compressive strength in a noticeable way. Lee et al. [12] concluded that raster angle, air gap and layer thickness influence the elastic performance of flexible ABS objects. Also Anitha et al. [13] studied the effect of the layer thickness showing that the performance increases when the thickness decreases. Sood et al. [14], using the response surface methodology, analyse the functional relationship between specimens strength and several factors, e.g., build orientation, layer thickness, raster angle and air gap. Their results show that these factors influence the bonding and distortion within the parts. Lee et al. [15] carried out several experiments on cylindrical layered parts made from three different rapid prototyping processes, i.e., FDM, 3D printer and nano-composite deposition (NCDS). The aim of their work was to study the effect of the build direction on the compressive strength. The results show that compressive strength is greater for axial FDM specimens than for the transverse ones. This empirical approach allows to understand easily the relation between the FDM process parameters and the mechanical properties of the material, but it needs expensive experimental campaigns and, generally, it is difficult to extrapolate the behaviour of the material in other conditions. On the contrary, few papers in literature deal with the development of predictive models to determine the mechanical properties of FDM parts. Croccolo et al. [16] develop an analytical model taking into account some of the 3D printer parameters to determine the final mechanical characteristics of the specimens. However, this model needs to introduce adhesive force between the beads that could be difficult to estimate. Contrariwise, the use of models widely known and implemented, such as the classical laminate theory, already employed for composite materials, could be a real advantage in terms of usability.

The aim of this work is to describe the mechanical behaviour of FDM parts by the classical laminate theory (CLT). In order to reach this objective, the values of the elastic modulus in the longitudinal and transverse directions to the fibre (E_1, E_2), the Poisson's modulus (ν_{12}) and the shear modulus (G_{12}) will be experimentally measured. The determination of E_1 and E_2 will be carried out by single layer tests conducted on specimens with 0° and 90° raster angles. The Poisson's modulus will be determined measuring, on five layers 0° specimens, the longitudinal and transverse deformation by strain gauges. The shear modulus, G_{12}, will be determined according to the ASTM D3518. In this study, two different material ABS and PLA will be employed to prove the validity of CLT on several materials.

2. Materials and methods

In this work the CLT has been applied to describe the mechanical behaviour of FDM printed parts. As requested by CLT, the values of the elastic modulus in the longitudinal and transverse directions to the fibre (E_1, E_2), the shear modulus (G_{12}) and the Poisson's modulus (ν_{12}) have been experimentally determined. Finally, the comparison between the CLT and the experimental results, conducted on ABS and PLA, has been carried out on symmetric and balanced specimens.

2.1. ***Classical Laminate Theory***

The classical laminate theory allows to calculate the elastic behaviour of a multi-layer orthotropic material using the constants that describe the mechanical behaviour of the single layer E_1, E_2, ν_{12}, G_{12} and h_c. E_1 and E_2 are the elastic modulus in the longitudinal and transverse directions to the fibre, ν_{12} is the Poisson's ratio, G_{12} is the shear modulus and h_c is the layer thickness. The reduced stiffness tensor $\mathbf{Q}_k$ can be calculated, for each layer k and in the layer system reference $\{x_1, x_2, x_3\}$ (Figure 1), as:

$$\boldsymbol{Q}_k = \begin{bmatrix} Q_{11} & Q_{12} & 0 \\ Q_{12} & Q_{22} & 0 \\ 0 & 0 & Q_{66} \end{bmatrix} \tag{1}$$

The terms in the matrix are:

$$Q_{11} = \frac{E_1}{1 - \upsilon_{12}\upsilon_{21}}, \quad Q_{12} = \frac{\upsilon_{21}E_1}{1 - \upsilon_{12}\upsilon_{21}}, \quad Q_{22} = \frac{E_2}{1 - \upsilon_{12}\upsilon_{21}}, \qquad Q_{66} = G_{12} \tag{2}$$

with

$$\upsilon_{21} = \upsilon_{12}\frac{E_2}{E_1} \tag{3}$$

The relations between the applied forces **N** and moments **M** and the resulting mid-plane strains $\boldsymbol{\varepsilon}^0$ and curvatures $\boldsymbol{\chi}$ can be summarized as a single matrix equation:

$$\begin{Bmatrix} \boldsymbol{N} \\ \boldsymbol{M} \end{Bmatrix} = \begin{bmatrix} \boldsymbol{A} & \boldsymbol{B} \\ \boldsymbol{B} & \boldsymbol{D} \end{bmatrix} \begin{Bmatrix} \boldsymbol{\varepsilon}^0 \\ \boldsymbol{\chi} \end{Bmatrix} \tag{4}$$

where the tensors **A**, **B** and **D**, when thickness h_c of the layers is constant, are:

$$\begin{gathered} \boldsymbol{A} = \frac{h}{n}\sum_{k=1}^{n} \boldsymbol{Q}_k(\delta_k) \\ \boldsymbol{B} = \sum_{k=1}^{n} \frac{1}{2}\frac{h^2}{n^2} b_k \boldsymbol{Q}_k(\delta_k) \\ \boldsymbol{D} = \sum_{k=1}^{n} \frac{1}{12}\frac{h^3}{n^3} d_k \boldsymbol{Q}_k(\delta_k) \end{gathered} \tag{5}$$

In eq. (5), k has been numbered from the bottom of the laminate, n is the total number of layers, h is the laminate thickness while b_k and d_k are:

$$b_k = 2k - n - 1 \tag{6}$$

$$d_k = 12k(k - n - 1) + 4 + 3n(n + 2) \tag{7}$$

In (5) $\boldsymbol{Q}_k(\delta_k)$ is the reduced stiffness tensor of the layer k in the laminate reference {x, y, z}. As indicated in Figure 1, δ_k is the angle between x-axis of the laminate reference and the x_1-axis of the layer k.

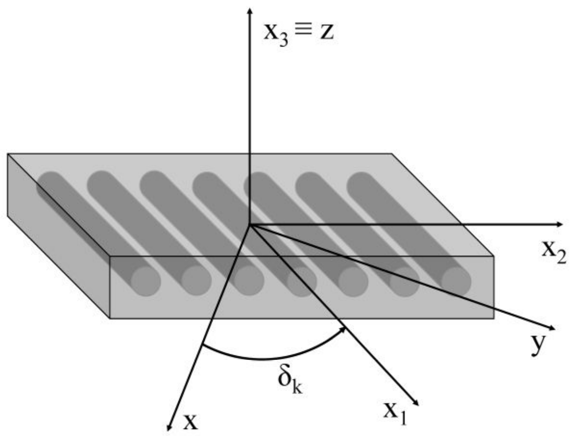

Figure 1 Laminate {x, y, z} and layer {x_1, x_2, x_3} systems reference

The calculation of the stress in each layer requires the calculation of the deformations and, thus, it is necessary to invert the laminate equation (4):

$$\begin{Bmatrix} \boldsymbol{\varepsilon}^0 \\ \boldsymbol{\chi} \end{Bmatrix} = \begin{bmatrix} \boldsymbol{A} & \boldsymbol{B} \\ \boldsymbol{B} & \boldsymbol{D} \end{bmatrix}^{-1} \begin{Bmatrix} \boldsymbol{N} \\ \boldsymbol{M} \end{Bmatrix} \tag{8}$$

Because this inversion could be quite complicate, another way to tackle the problem is to reverse one by one the three tensors that appear in (8), A, B and D. Thus, it is possible to rewrite (8) in the form:

$$\begin{Bmatrix} \boldsymbol{\varepsilon}^0 \\ \boldsymbol{\chi} \end{Bmatrix} = \begin{bmatrix} \boldsymbol{a} & \boldsymbol{b} \\ \boldsymbol{b}^T & \boldsymbol{d} \end{bmatrix}^{-1} \begin{Bmatrix} \boldsymbol{N} \\ \boldsymbol{M} \end{Bmatrix} \quad (9)$$

with

$$\boldsymbol{a} = (\boldsymbol{A} - \boldsymbol{B}\boldsymbol{D}^{-1}\boldsymbol{B})^{-1}$$
$$\boldsymbol{d} = (\boldsymbol{D} - \boldsymbol{B}\boldsymbol{A}^{-1}\boldsymbol{B})^{-1} \quad (10)$$
$$\boldsymbol{b} = -\boldsymbol{a}\boldsymbol{B}\boldsymbol{D}^{-1} = -(\boldsymbol{A} - \boldsymbol{B}\boldsymbol{D}^{-1}\boldsymbol{B})^{-1}\boldsymbol{B}\boldsymbol{D}^{-1}$$

Finally, in order to obtain the laminate properties, it can be defined:

$$\boldsymbol{a}^* = h\boldsymbol{a} \quad (11)$$

Thus, the laminate Young's Modulus in the x direction is:

$$E_x = \frac{1}{a_{11}^*} \quad (12)$$

In order to demonstrate the usefulness of employing the CLT to model the FDM structures, this value of the laminate Young's modulus will be compared with that measured experimentally.

2.2. *Experimental procedure*

A RepRap Prusa i3 equipped with a marlin firmware and a nozzle with a diameter of 0.4 mm has been employed for the production of the specimens. Some parameters, such as the layer thickness or the number of contour lines, have been kept constant for every specimen. These values have been reported in Table 1. The bed temperature for ABS has been set to 90 °C and to 55 °C for PLA. Moreover, the nozzle temperature is 225 °C for ABS and 200 °C for PLA. Finally, the specimens have been fabricated with the minimum dimension of the part perpendicular to the build platform.

Table 1 Fixed printer parameters

Parameter	Value
Air gap [mm]	0
Layer thickness [mm]	0.35
Bead width [mm]	0.70
Number of contour lines	2

In Table 1, the air gap is the distance between two, adjacently deposited, beads of the same layer; the layer thickness and the bead width are respectively the height and the width of a deposited filament. The number of contours represents how many edges have been deposited before filling the inner part by inclined beads. The angle, relative to the load direction, with which the beads are deposited is called the raster angle (e.g. 0° raster angle layer has deposited with beads parallel to the load direction). The samples have been shaped as required by the standard ASTM D638-10 with reference to the geometry of the first typology (Figure 2). The solid model, created using a 3D CAD, has been sliced using the open source software Slic3r.

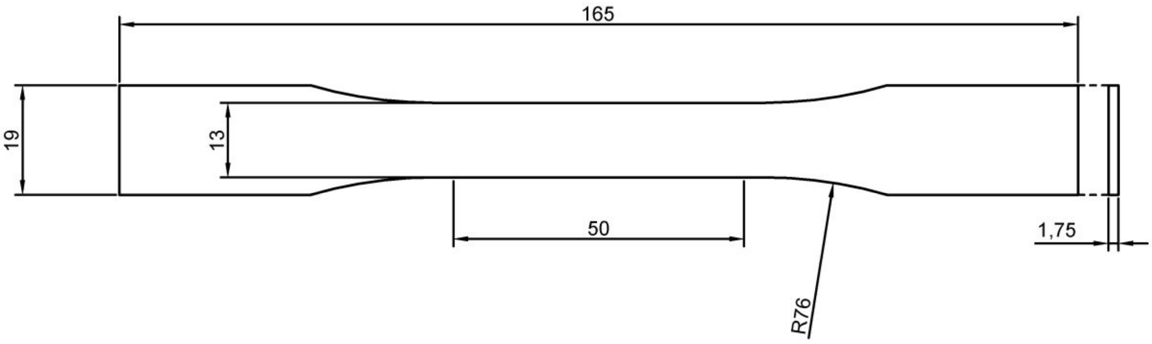

Figure 2 ASTM D638 Specimen shape with dimensions in mm

Five specimens for each direction and material have been made for the experimental measure of the elastic modulus of the single layer in the longitudinal and transverse directions to the fibre (E_1, E_2). The Figure 3 shows a detail of single layer ABS specimen (Figure 3a) with a raster angle of 90° and a detail of single layers PLA specimen (Figure 3b) with a raster angle of 0°. In addition, 45° specimens have been made in order to show in a better way the orthotropic mechanical behaviour of FDM specimens (Figure 3c). The tensile tests have been carried out on an Instron 3343 equipped with a 1000 N load cell and ISO 9513 class 0.5 extensometer. A crosshead speed of 5 mm/min has been selected according with ASTM D638-10.

The Poisson's modulus (ν_{12}) has been measured on five layers 0° specimens due to the difficulty to measure the transversal strain on single layer specimen. The longitudinal and transverse deformations have been measured using strain gauges and a HBM QuantumX 840 has been employed to acquire the data.

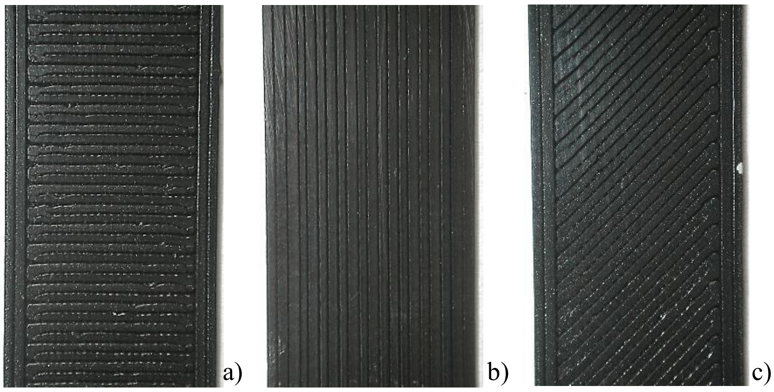

Figure 3 A detail of the single layer specimens: a) 90° orientation specimen; b) 0° orientation specimen; c) 45° orientation specimen.

The shear modulus (G_{12}) has been measured according with ASTM D3518-94. For each material, three flat rectangular specimens have been made with dimension 200 mm length, 25 mm width and 5.6 mm thick. These samples consists of 16 layers in a symmetric criss-cross configuration, i.e. the stack sequence is $[+45/-45]_{4s}$. The tests have been carried out on a MTS Alliance RT/30 instrumented with a 30 kN load cell. According with ASTM D3518-94 a crosshead speed of 2 mm/min has been used during the test.

In order to compare the CLT and the experimental results, five specimens for each material have been made with a symmetric and balanced stack sequence [+30/-30/0/-30/+30]. The ABS specimens have been tested on Instron 3343. However, because the PLA samples are stronger than the ABS ones and they would be broken at higher load than 1000 N, a MTS Alliance RT/30 with a 30 kN load cell has been used for the PLA tests. The stain measurements has been acquired using an MTS 634.25F-54.

3. Results

The result data have been processed, following the recommendations of ASTM D638-10, for the determination of the Young's modulus E and the ultimate tensile strength UTS values. The Young's modulus E has been determined considering the linear part of the stress–strain curve and the slope has been estimated by a linear fit. The UTS has been calculated as a ratio between the maximum load reached during the test and the cross-sectional area. The mechanical properties for the two feedstock wire materials have been experimentally determined and reported in Table 2 and Table 3. The tests on the wire show that the PLA has a Young's modulus and UTS values that are about twice the values of ABS. However, even if PLA is stronger than ABS it is more brittle. Indeed, the deformation at fracture is 0.079 mm/mm for the PLA and 0.16 mm/mm for the ABS. Moreover, the most important disadvantages of PLA compared to ABS are the lower capacity to stand temperature higher that room temperature and the lower durability due to its biodegradability. A summary of the average results for the single layer tensile tests has been reported in Table 2 for ABS and Table 3 for PLA.

Table 2 ABS Single layer mechanical properties at different raster angle

Specimen	**Young's modulus [GPa]**	**Young's modulus Standard deviation [GPa]**	**UTS [MPa]**	**UTS Standard deviation [MPa]**
ABS Wire	1.81	0.18	32.11	0.30
ABS 0°	1.79	0.58	26.11	2.37
ABS 45°	1.38	0.11	11.97	3.12
ABS 90°	1.15	0.09	6.71	0.36

Table 3 PLA Single layer mechanical properties at different raster angle

Specimen	**Young's modulus [GPa]**	**Young's modulus Standard deviation [GPa]**	**UTS [MPa]**	**UTS Standard deviation [MPa]**
PLA Wire	3.38	0.05	55.26	0.76
PLA 0°	3.12	0.03	50.23	0.77
PLA 45°	2.86	0.02	40.68	0.75
PLA 90°	2.77	0.32	22.49	6.75

The Table 2 and Table 3 show that the wire, both for PLA and ABS, are stiffer and stronger than the 0° single layer samples. This is probably due to the extrusion process that influence, introducing some defects, the resulting specimens. Moreover, the single layer tests highlights the orthotropic behaviour of the FDM parts showing a reduction of the mechanical characteristics increasing the raster angle. The mean Young's modulus decreases between 0° and 90° of 35.72% for ABS and 11.12% for PLA. The mean UTS shows a reduction of 74.30% for ABS and of 55.22% for PLA. This trend suggests that ABS has a much more marked orthotropic behaviour than PLA. Probably, this is due to a better capacity of PLA to bond each bead to the other. The 45º specimens have an intermediate behaviour between the 0° and 90° mechanical properties. However, for both ABS and PLA, the 45° behaviour is nearer to 90° than 0°. Some representative stress-strain curves have been reported for the single layer specimens changing the raster angle in Figure 4 for ABS and Figure 5 for PLA.

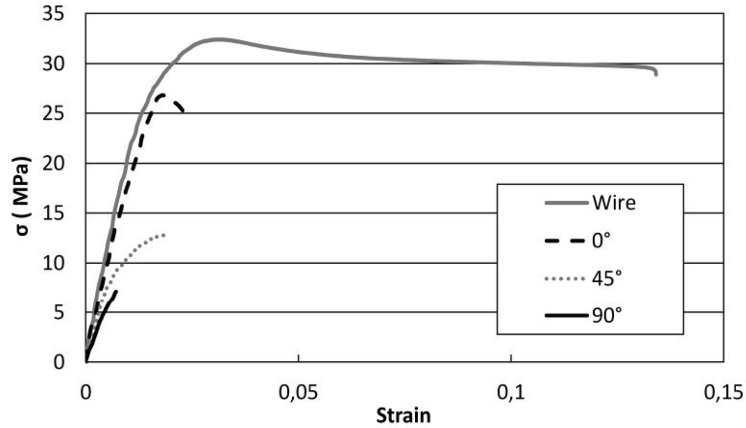

Figure 4 Representative tensile testing data for ABS at each raster orientation

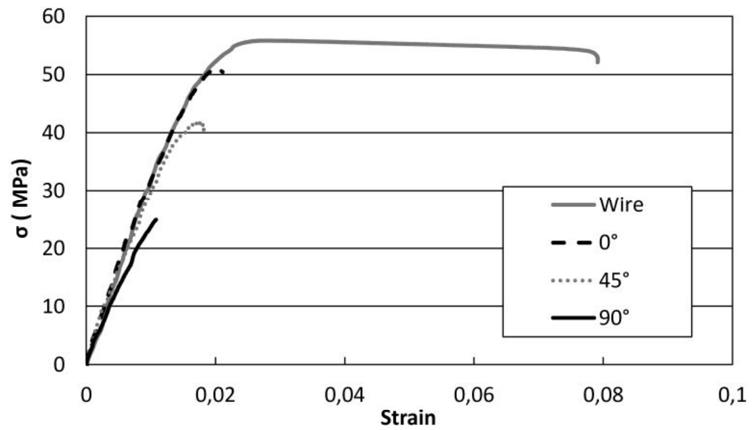

Figure 5 Representative tensile testing data for PLA at each raster orientation

In general, the results highlight a brittle behaviour for FDM specimens compared to the feedstock wire. However, 45° and 0° specimens show a little plastic behaviour compared to the 90° specimens that have a perfect brittle trend without plastic deformation. These results, showing the orthotropic properties of FDM specimens, confirm that the raster orientation has an important effect on the tensile strength, the Young's modulus and deformation at fracture.

In Figure 6, some representative shear stress vs. shear strain curves have been reported. As recommended by ASTM D3518-94, the slope of the curve between the point with a deformation of 2000 $\mu\varepsilon$ and 6000 $\mu\varepsilon$ is the shear modulus G_{12}. The mean vales of G_{12} obtained for PLA is 1246.57 ± 32.21MPa and 808.58 ± 17.80 MPa for ABS.

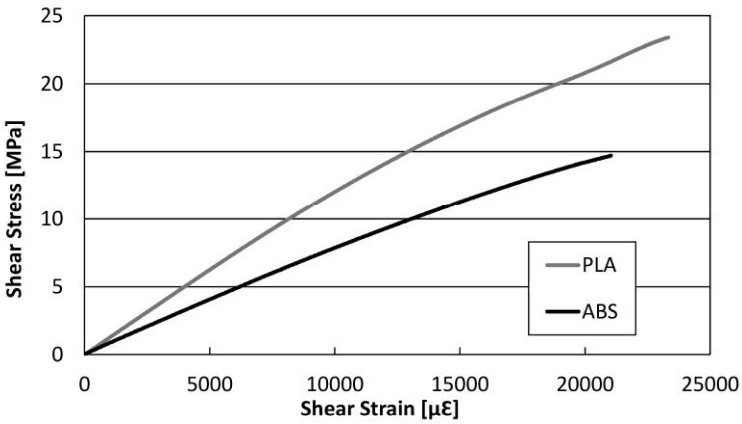

Figure 6 Representative shear stress - shear strain data for both PLA and ABS

Figure 7a for ABS and Figure 7b for PLA, show the comparison between experimental stress-strain curves of [+30/-30/0/-30/+30] specimens and CLT. In these figures, the dotted line represents the elastic modulus predicted by CLT. The values are 1.88 GPa for ABS and 3.17 GPa for PLA and these have been calculated using the measured Poisson's modulus of 0.344 for ABS and 0.330 for PLA. The mean experimental values are 1.86 ± 0.075 GPa for ABS and 3.35 ± 0.095 GPa for PLA. In Figure 7c a comparison between experimental elastic modulus and CLT prediction has been reported. The difference between CLT and experimental vales are 1.07% for ABS and 5.37% for PLA. Finally, the mean UTS are 32.18 ± 0.47 MPa for ABS and 55.37 ± 1.44 MPa for PLA.

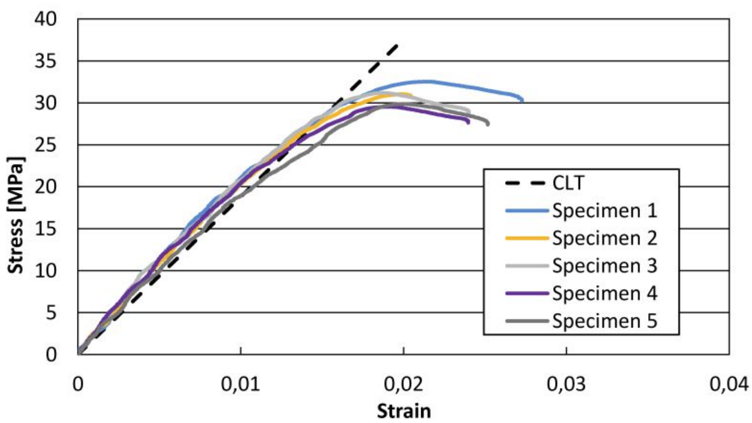

a

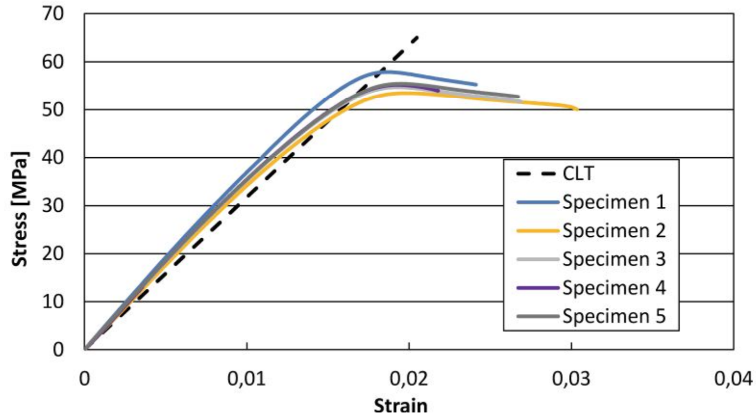

b

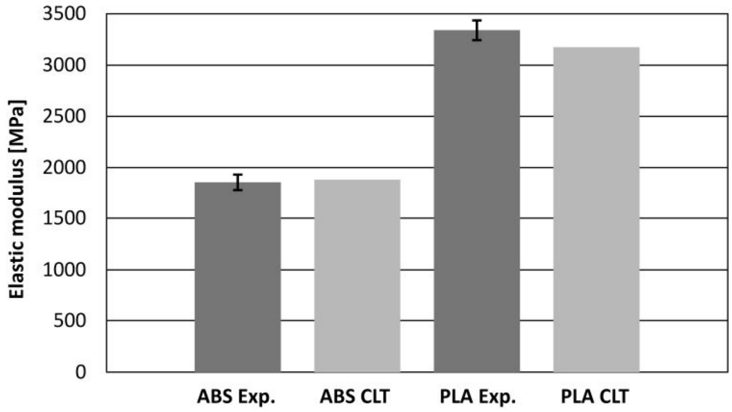

c

Figure 7 Experimental data vs. CLT for Abs (a) PLA (b) and comparison between elastic modulus (c)

4. Conclusion

In this paper, the mechanical behaviour of FDM parts has been described using the classical laminate theory (CLT). In view of this aim, some mechanical parameters employed in CLT has been experimentally determined. The values of the Young's modulus in the longitudinal and transverse directions to the fibre (E_1, E_2) has been carried out by single layer tests conducted on specimens with 0° and 90° raster angles. The shear modulus (G_{12}) has been determined according to the ASTM D3518. The Poisson's modulus have been measured on five layers 0° specimens acquiring the longitudinal and transverse deformation by strain gauges. The comparison between the CLT and the experimental results have been carried out on specimens with a symmetric and balanced stack sequence [+30/-30/0/-30/+30]. Finally, two different material, ABS and PLA, have been employed to prove the validity of CLT prediction on several materials.

The tests on the wire show that the PLA has a Young's modulus and UTS values that are about twice the values of ABS even if it is more brittle. For both PLA and ABS, the wire are stiffer and stronger than the 0° single layer samples and this is probably due to the extrusion process that introduces some defects in the resulting specimens. The experimental results highlight the orthotropic behaviour of FDM specimens showing a reduction of the mechanical characteristics increasing the raster angle. The Young's modulus, increasing the raster angle from 0° to 90°, decreases of 35.72% for ABS and 11.12% for PLA. Moreover, the mean UTS shows a reduction of 74.30% for ABS and of 55.22% for PLA changing the raster angle. Apparently, these results suggest that ABS has more marked orthotropic behaviour than PLA. One of the potential motivation of this PLA behaviour should be a better capacity of this material to bond each bead to the other. In addition, tests on 45° specimens have been carried out. For both materials analysed, the 45º specimens have an intermediate mechanical behaviour between the 0° and 90° even if the mechanical behaviour is nearer to 90° than 0°.

The CLT has showed a high capacity to predict the elastic modulus of ABS and PLA laminate obtained by FDM. Furthermore, the results are in according with other models present in literature [16], that showed higher errors between experimental results and model prediction (from -4.7% to 6.6%).

Reference

1. Caulfield, B., P.E. McHugh, and S. Lohfeld, *Dependence of mechanical properties of polyamide components on build parameters in the SLS process.* Journal of Materials Processing Technology, 2007. **182**(1–3): p. 477-488.
2. Chua, C.K., S.M. Chou, and T.S. Wong, *A study of the state-of-the-art rapid prototyping technologies.* The International Journal of Advanced Manufacturing Technology, 1998. **14**(2): p. 146-152.
3. Yan, X. and P. Gu, *A review of rapid prototyping technologies and systems.* Computer-Aided Design, 1996. **28**(4): p. 307-318.
4. Stephens, B., et al., *Ultrafine particle emissions from desktop 3D printers.* Atmospheric Environment, 2013. **79**(0): p. 334-339.
5. Zein, I., et al., *Fused deposition modeling of novel scaffold architectures for tissue engineering applications.* Biomaterials, 2002. **23**(4): p. 1169-1185.
6. Zhong, W., et al., *Short fiber reinforced composites for fused deposition modeling.* Materials Science and Engineering: A, 2001. **301**(2): p. 125-130.
7. Allahverdi, M., et al., *Processing of advanced electroceramic components by fused deposition technique.* Journal of the European Ceramic Society, 2001. **21**(10–11): p. 1485-1490.
8. Mireles, J., et al., *Development of a Fused Deposition Modeling System for Low Melting Temperature Metal Alloys.* Journal of Electronic Packaging, 2013. **135**(1): p. 011008-011008.
9. Masood, S.H. and W.Q. Song, *Development of new metal/polymer materials for rapid tooling using Fused deposition modelling.* Materials & Design, 2004. **25**(7): p. 587-594.
10. Tymrak, B.M., M. Kreiger, and J.M. Pearce, *Mechanical properties of components fabricated with open-source 3-D printers under realistic environmental conditions.* Materials & Design, 2014. **58**: p. 242-246.

11. Ahn, S.-H., et al., *Anisotropic material properties of fused deposition modeling ABS.* Rapid Prototyping Journal, 2002. **8**(4): p. 248-257.

12. Lee, B.H., J. Abdullah, and Z.A. Khan, *Optimization of rapid prototyping parameters for production of flexible ABS object.* Journal of Materials Processing Technology, 2005. **169**(1): p. 54-61.

13. Anitha, R., S. Arunachalam, and P. Radhakrishnan, *Critical parameters influencing the quality of prototypes in fused deposition modelling.* Journal of Materials Processing Technology, 2001. **118**(1–3): p. 385-388.

14. Sood, A.K., R.K. Ohdar, and S.S. Mahapatra, *Parametric appraisal of mechanical property of fused deposition modelling processed parts.* Materials & Design, 2010. **31**(1): p. 287-295.

15. Lee, C.S., et al., *Measurement of anisotropic compressive strength of rapid prototyping parts.* Journal of Materials Processing Technology, 2007. **187–188**(0): p. 627-630.

16. Croccolo, D., M. De Agostinis, and G. Olmi, *Experimental characterization and analytical modelling of the mechanical behaviour of fused deposition processed parts made of ABS-M30.* Computational Materials Science, 2013. **79**(0): p. 506-518.